J. theor. Biol. (1999) **198,** 101–120
Article No. jtbi.1999.0905, available online at http://www.idealibrary.com on IDEAL

Stochastic Model of Central Synapses: Slow Diffusion of Transmitter Interacting with Spatially Distributed Receptors and Transporters

JULIA TROMMERSHÄUSER*, JÖRG MARIENHAGEN AND ANNETTE ZIPPELIUS

Institut für Theoretische Physik, Georg-August Universität Göttingen, Bunsenstraße 9, 37073 *Göttingen, Germany*

(*Received on* 18 *August* 1998, *Accepted in revised form on* 7 *January* 1999)

A detailed mathematical analysis of the diffusion process of neurotransmitter inside the synaptic cleft is presented and the spatio-temporal concentration profile is calculated. Using information about the experimentally observed time course of glutamate in the cleft the effective diffusion coefficient D_{net} is estimated as $D_{net} \sim 20$–$50\ \mathrm{nm}^2\ \mu\mathrm{s}^{-1}$, implying a strong reduction compared with free diffusion in aqueous solution. The tortuosity of the cleft and interactions with transporter molecules are assumed to affect the transmitter motion. We estimate the transporter density to be 5170 to 8900 $\mu\mathrm{m}^{-2}$ in the synaptic cleft and its vicinity, using the experimentally observed time constant of glutamate. Furthermore a theoretical model of synaptic transmission is presented, taking the spatial distribution of post-synaptic (AMPA-) receptors into account. The transmitter diffusion and receptor dynamics are modeled by Monte Carlo simulations preserving the typically observed noisy character of post-synaptic responses. Distributions of amplitudes, rise and decay times are calculated and shown to agree well with experiments. Average open probabilities are computed from a novel kinetic model and are shown to agree with averages over many Monte Carlo runs. Our results suggest that post-synaptic currents are only weakly potentiated by clustering of post-synaptic receptors, but increase linearly with the total number of receptors. Distributions of amplitudes and rise times are used to discriminate between different morphologies, e.g. simple and perforated synapses. A skew in the miniature amplitude distribution can be caused by multiple release of pre-synaptic vesicles at perforated synapses.

1. Introduction

Differences in the processing of information at synapses of the central nervous system (CNS) and at synapses of the neuromuscular junction (NMJ) are not surprising, given the different ways of functioning of the two systems. NMJ synapses are larger in size, have a higher number of receptors and exhibit a wider synaptic cleft. At central synapses (see Edwards, 1995b for a review) the synaptic cleft is not only much narrower (e.g. Ichimura & Hashimoto, 1988), but also seems to be filled with several molecules or a dense staining, gel-like material (see e.g. Edwards, 1995b; Harris & Kater, 1994; Peters & Kaiserman-Abramof, 1969; Van der Loos, 1963). The amount of transmitter molecules released at CNS synapses exceeds the number of post-synaptic receptors by far, suggesting mechanisms of plasticity different from those at the NMJ (see e.g. Bekkers, 1994; Edwards, 1995b).

*Author to whom correspondence should be addressed.
E-mail: trommer@theorie.physik.uni-goettingen.de

0022–5193/99/009101 + 20 $30.00/0

Furthermore synapses of the CNS show a surprising morphological variety whose effects for the function of synaptic transmission and plasticity is not understood.

Several theoretical approaches to modelling synaptic transmission have been introduced and proven useful to elucidate mechanisms of synaptic transmission at the NMJ (Agmon & Edelstein, 1997; Bartol *et al*., 1991; Bennett *et al*., 1995, 1997; Faber *et al*., 1992; Stiles *et al*., 1996) as well as at CNS synapses (Barbour *et al*., 1994; Busch & Sakmann, 1990; Holmes, 1995; Kleinle *et al*., 1996; Kruk *et al*., 1997; Marienhagen & Zippelius, 1995; Uteshev & Pennefather, 1996, 1997; Wahl *et al*., 1996). All these models involve free parameters which either have not been determined experimentally or are not accessible. For example the diffusion coefficient of glutamate has only been measured in aqueous solution (Longworth, 1953) and not in the cleft. The values assigned to this parameter in various models of synaptic transmission vary from $10\,\mathrm{nm^2\,\mu s^{-1}}$ (Kleinle *et al*., 1996) to $760\,\mathrm{nm^2\,\mu s^{-1}}$ (Barbour *et al*., 1994), corresponding to its value in aqueous solution. Assumptions regarding mechanisms of transmitter release (see e.g. Kleinle *et al*., 1996) and uptake (see e.g. Holmes, 1995; Rusakov & Kullmann, 1998; Uteshev & Pennefather, 1997) also differ remarkably.

Being aware of the large number of poorly known model parameters we design a theoretical model of excitatory, glutamate AMPA-mediated synaptic transmission using the *minimal number of free parameters* necessary to account for the basic features of the transmission process.

In a first step we will estimate a *net-diffusion coefficient* D_{net} to characterize the net-dynamics of transmitter molecules, using the knowledge about transmitter–transporter interactions (Wadiche *et al*., 1995; Diamond & Jahr, 1997) and the total residence time of transmitter molecules inside the cleft (from Clements *et al*., 1992). We use the diffusion equation to model the net-movement of transmitter molecules inside the synaptic cleft, which is most likely slowed down compared with aqueous solution due to multiple binding and unbinding effects to transporters within the cleft and its vicinity (see e.g. Asztely *et al*., 1997; Bergles & Jahr, 1997; Diamond & Jahr, 1997; Edwards, 1995b; Isaacson & Nicoll, 1993; Mennerick *et al*., 1998; Otis *et al*., 1997; Takahashi *et al*. 1996; Tong and Jahr, 1994a, b; Wang *et al*., 1998). We show that concentration fluctuations equilibrate rapidly across the height of the synaptic cleft, so that a two-dimensional profile is sufficient to account for spatial fluctuations in transmitter concentration. From the concentration profile of our model, we calculate the average residence time of transmitter molecules in the cleft and compare it to the experimentally observed time (Clements *et al*., 1992). This yields an estimate of the net-diffusion coefficient of $D_{net} = 20$–$50\,\mathrm{nm^2\,\mu s^{-1}}$.

In a second step we use a Monte Carlo model as first introduced by Bartol *et al*. (1991) in this context, with the purpose to discuss and to reproduce the ''noisy'' shape of post-synaptic currents due to the inherent noise in the individual receptor dynamics (see e.g. Jonas *et al*., 1993; Spruston *et al*., 1995; Hausser & Roth, 1997). We compute the distribution of amplitudes, rise and decay times of AMPA mediated EPSCs, which turn out to be as broad as observed experimentally (Jonas *et al*., 1993; Spruston *et al*., 1995).

In a third step we derive a novel chemical kinetic scheme describing individual, spatially distributed post-synaptic receptors in a locally changing concentration field. The model is based on the assumption that variations in the transmitter concentration due to binding and unbinding by post-synaptic receptors can be neglected. Since the number of post-synaptic receptors is low compared with the number of transmitter molecules released, this assumption is well justified at CNS synapses. Chemical kinetics provides a very fast and accurate scheme to calculate average properties and investigate the influence of different receptor distributions on the shape of EPSCs. We focus on AMPA-/kainate receptors, which are thought to mediate the large component of excitatory post-synaptic currents (see Edmonds *et al*., 1995, for a review). They exhibit a lower binding affinity for glutamate than NMDA receptors, which should lead to a higher sensitivity of AMPA-/kainate responses due to spatial fluctuations in the receptor distribution or in the

transmitter concentration (see e.g. Kullmann & Asztely, 1998).

2. Theoretical Model

2.1. DIFFUSION OF NEUROTRANSMITTER IN THE SYNAPTIC CLEFT

We model the synaptic cleft as a flat cylinder [Fig. 1(a)], because pre- and post-synaptic terminals stick together closely in central synapses. The transmitter is released from a point source at the pre-synaptic side of the cleft* and spreads inside the cylindrical cleft according to Fick's second law. Certainly the transmitter movement inside the cleft is different from free diffusion in aqueous solution due to interactions with transporters or a dense, gel-like material (see e.g. Edwards, 1995b; Harris & Kater, 1994). The effects of these interactions are two-fold: first, frequent fast binding of transmitter to transporters and other molecules, as well as the tortuosity of the cleft, will slow down diffusion, but will not remove transmitter irreversibly from the cleft. Hence the transmitter dynamics remains diffusive for time-scales relevant to the receptor kinetics and is modeled by a net diffusion coefficient D_{net}, smaller than the free diffusion coefficient D_{water}. For a particular kinetic scheme of transmitter–transporter interaction (Diamond & Jahr, 1997; Wadiche *et al*., 1995) we compute the time course of glutamate in the cleft and estimate the density of transporters in the cleft and its vicinity. Second, uptake and transport into intracellular compartments causes depletion of transmitter. Although detailed information about the distribution and density of transporters in- and outside the cleft is not available so far, there seems to be agreement about the existence of intra- and extra-synaptic uptake mechanisms to ensure glial and neuronal uptake and a rapid clearance of abundant transmitter molecules (Bergles & Jahr, 1997; Hertz *et al*., 1978; Holmes, 1995; Kullmann & Asztely, 1998; Rusakov & Kullmann, 1998; Takahashi *et al*., 1996; Wang *et al*., 1998). We model neuronal and glial transmitter uptake by introducing an absorbing boundary for the diffusion field. Its location is chosen outside the post-synaptic density (PSD), which contains the post-synaptic receptors and typically exhibits a diameter of 100 to 400 nm (see

*There has been a discussion in the literature about the effect of diffusion pores on transmitter diffusion (see e.g. Khanin *et al*., 1994; Holmes, 1995; Kleinle *et al*., 1996; Clements, 1996; Uteshev & Pennefather, 1996). As the authors come to differing conclusions about the necessity of including a diffusion pore into theoretical modeling, we want to restrict our model to the simplest case for the beginning.

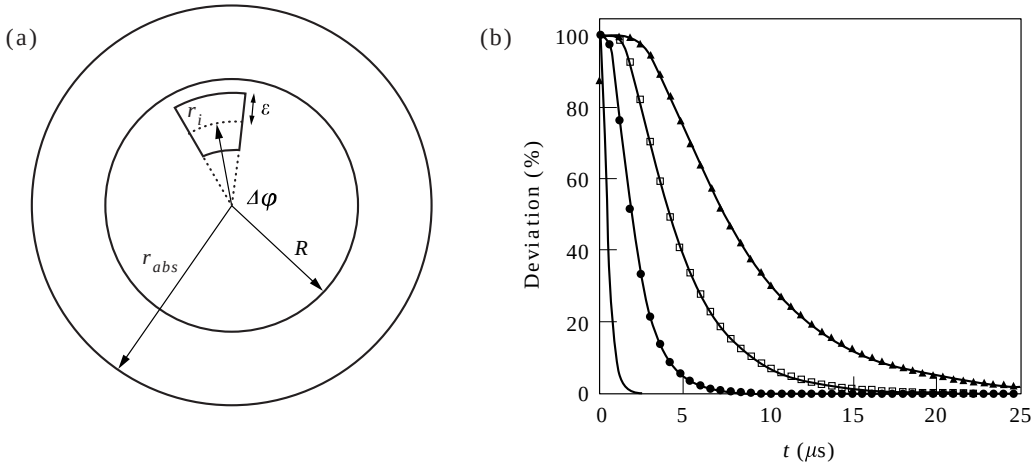

FIG. 1. (a) Two-dimensional model of the synaptic disc: post-synaptic receptors are distributed within the PSD of radius R. Once the transmitter molecules hit r_{abs} they are absorbed. Small area increment $\Delta F = 2\varepsilon r_i \Delta\varphi = 2(\varepsilon)^2$, bounded by $\Delta\varphi$ and 2ε to estimate the local transmitter concentration for a receptor located at position $\mathbf{r}_i$; (b) difference Λ between a two- and a three-dimensional model of the synaptic cleft as function of time and for different heights h of the synaptic cleft. The three-dimensional model is averaged over the small interval of height $\delta = 5$ nm. (——) $h = 10$ nm; (●) $h = 20$ nm; (□) $h = 30$ nm; (▲) $h = 40$ nm.

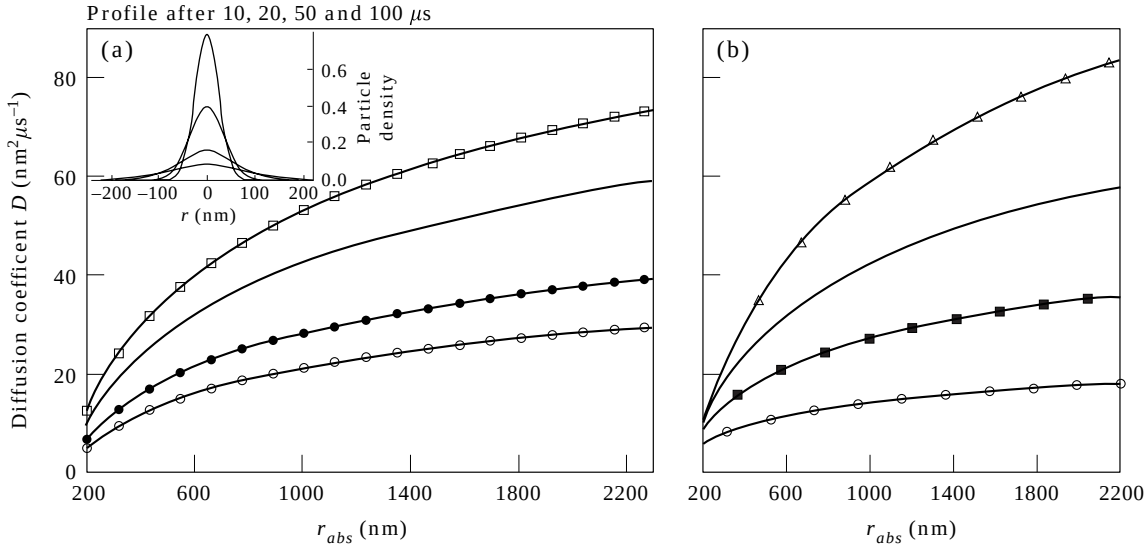

FIG. 2. Estimate of the net-diffusion coefficient D_{net} as a function of the model parameter r_{abs}. (a) The spatio-temporal concentration profile (small upper inset) is averaged over time and area of the PSD. The diffusion coefficient D_{net} is shown for $R = 200$ nm and several estimates of $\langle T \rangle$: (□) 0.8 ms; (——) 1 ms; (●) 1.5 ms; (○) 2 ms. Upper inset: concentration profile as function of the radial component r as calculated from eqn (A.2), at times $t = 10$, 20, 50 and 100 μs; transmitter release in the middle of the synaptic disc; (b) estimate of D_{net} for $\langle T \rangle = 1$ ms and different radii of the PSD [$R = 100$ (○), 150 (■), 200 (——) and 250 (△) nm).

e.g. Edwards, 1995b), so that the absorbing boundary is set in the range of 500 to 1000 nm [Fig. 1(a)], i.e. comparable to the typical distance between neighboring synapses (Rusakov & Kullmann, 1998). An absorbing boundary at larger distances has the same effect as less efficient uptake mechanisms (see Fig. 3).

Given the boundary and initial conditions introduced above, the three-dimensional spatio-temporal concentration profile $c(r,\varphi,z,t)$ of transmitter molecules in the cleft can be computed (see Appendix A.1). Since the extension $h \sim 15$–20 nm of the synaptic cleft in the z-direction is small compared with its extension in the lateral direction, it is reasonable to reduce the model to two dimensions (see Appendix A.2). The three-dimensional concentration profile is integrated over a small distance δ right above the PSD and compared with the two-dimensional profile $c_\Phi(r,\varphi,t)$ in Fig. 1(b): the differences are seen to vanish within a few μs.

2.1.1. *Mean residence time of transmitter in the cleft*

The residence time $\langle T \rangle$ of a particle, which diffuses along the path $X(t)$, is given as the integral over all times, which the particle spends inside the area $K_R = \pi R^2$ of the PSD (for detailed calculations see Appendix A.1), i.e.

$$\begin{aligned}\langle T \rangle &= \int_0^\infty \mathrm{d}t\, \langle \Upsilon_{K_R}(X(t)) \rangle,\ \Upsilon_{K_R}(x) := \begin{cases} 1 & x \in K_R \\ 0 & \text{elsewhere} \end{cases} \\ &= \frac{1}{N_T} \int_0^\infty \mathrm{d}t \int_0^{2\pi} \mathrm{d}\varphi \int_0^R \mathrm{d}r\ r\ c_\Phi\ (r,\varphi,t) \\ &= \frac{2Rr_{abs}}{D_{net}} \sum_{n=1}^{\infty} \frac{1}{\lambda_{0n}^3} \frac{J_0(\alpha_{0n} r_0) J_1(\alpha_{0n} R)}{[J_1(\lambda_{0n})]^2}, \end{aligned} \tag{1}$$

with J_m denoting the m-th Bessel function of the first kind, λ_{mn} the n-th zero of J_m and $\alpha_{mn} = \lambda_{mn}/r_{abs}$. Hence eqn (1) relates the mean residence time $\langle T \rangle$ to the radius R of the PSD, the radius of the absorbing boundary r_{abs} and the net-diffusion coefficient D_{net}. Experiments on glutamatergic synapses yield the following estimates: $\langle T \rangle \sim 1$ ms for the residence time (Barbour *et al.*, 1994; Clements, 1992; Spruston *et al.*, 1995), $R \sim 200$ nm for the radius of the PSD (see e.g. Edwards, 1995b) and $r_{abs} \sim 500$–1000 nm (Rusakov & Kullmann, 1998). This leaves us with a range of values for D_{net} giving rise to the experimentally observed values of T, R and r_{abs} (see Fig. 2 and Table 1). The absorbing

TABLE 1
Range of parameters

Symbol	Definition	Value	Comment
Δt	Time step	4 μs	
Geometry			
h	Height synaptic cleft	15 nm	From Edwards (1995b)
R	Radius PSD	50–400 nm	From Edwards (1995a, b)
r_{abs}	Radius absorbing boundary	200–2000 nm	From Rusakov & Kullmann (1998)
ΔF	Binding area	113.1 nm^2	Free parameter, kinetic model
r_{bind}	"Binding radius"	6 nm	Free parameter, Monte Carlo simulation
Transmitter			
N_T	No. of molecules per vesicle	2000–4000	From Edwards (1995b)
T_{exp}, $\langle T \rangle$	Time constant	0.8–2 ms	From Clements (1992)

boundary is set in the range $R \leqslant r_{abs} \leqslant 10\,R$ which gives an estimate for $D_{net} \sim 20$–$50\ nm^2\ \mu s^{-1}$ (Fig. 2).

If the range of transmitter diffusion is unbounded ($r_{abs} = \infty$), i.e. no uptake is considered at all (as done e.g. by Barbour *et al*., 1994; Kleinle *et al*., 1996; Wahl *et al*., 1996), the concentration profile is given exactly by $c_\Phi(r,\varphi,t) = N_T\ \exp\ (-r^2/(4Dt))/(4\pi D_{net}t)$. The mean residence time is then infinite due to a logarithmic divergence of the integral in eqn (1) at long times and cannot be used to estimate D_{net}.

2.1.2. *The reduced diffusion coefficient reflects a large transporter density*

The calculated value of D_{net} is one order of magnitude smaller than the free diffusion coefficient of glutamate $D_{water} = 760\ nm^2\ \mu s^{-1}$ in water (Longworth, 1953) and indicates that the transmitter molecules in the cleft are slowed down compared with free diffusion in aqueous solution. A reduction of the diffusion coefficient to a value of $D_{net} \sim 300\ nm^2\ \mu s^{-1}$ due to tortuosity of the cleft has been suggested (Garthwaite, 1985; Nicholson & Phillips, 1981; Rise *et al*., 1985; Ichimura & Hashimoto, 1988). Several theoretical approaches have followed this idea (Barbour *et al*., 1994; Holmes, 1995; Uteshev & Pennefather, 1997; Wahl *et al*. 1996). The reduction which we find ($D_{net} \sim 30\ nm^2\ \mu s^{-1}$) is much stronger and in correspondence with Kleinle *et al*. (1996) and Bennett *et al*. (1997), who obtained reasonable time courses in calculated EPSCs using such a small diffusion coefficient as a fit parameter.

An increase in EPSC-amplitudes following the blocking of transporters has been observed (Barbour *et al*., 1994; Diamond & Jahr, 1997; Isaacson & Nicoll, 1993; Tong & Jahr, 1994a, b) and it has been suggested that first transporters buffer transmitter on a fast submillisecond time-scale (Diamond & Jahr, 1997), while the transport cycle itself is slow ($\sim 20\ s^{-1}$) compared with the AMPA-EPSC rise time (Wadiche *et al*., 1995; Diamond & Jahr, 1997). These findings are summarized in a kinetic scheme (Rusakov & Kullmann, 1998)

$$\mathrm{Tr} + \mathrm{B} \underset{v_2}{\overset{v_1}{\rightleftharpoons}} \mathrm{TrB} \overset{v_3}{\rightarrow} \mathrm{B}, \qquad (2)$$

with Tr denoting the transmitter, B the transporter, and TrB the transmitter–transporter complex. The second step models the depletion of transmitter due to transport into an intracellular compartment and the reappearance of the unbound transporter. This enables us to roughly estimate the effect of a given transporter density on the time course of the spatially averaged overall transmitter concentration in the cleft (Fig. 3).

As displayed in Fig. 3 buffering of transmitter by transporters as calculated from the kinetic scheme gives rise to transmitter dynamics

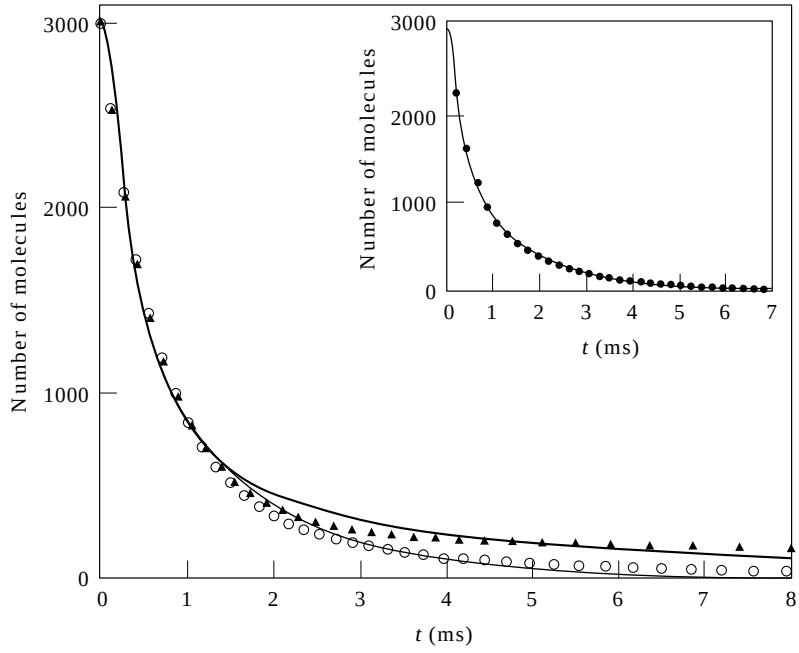

FIG. 3. Time course of 3000 transmitter molecules inside the PSD (radius $R = 200$ nm) as calculated from the net-diffusion model (transmitter release from a point source in the middle of the PSD, diffusion coefficient $D_{net} = 30\ \text{nm}^2\ \mu\text{s}^{-1}$, absorbing boundary at $r_{abs} = 500$ nm, black line, and $r_{abs} = 1000$ nm, thick black line). (▲) indicate the transmitter time course as caused by transporters (kinetic rates from Diamond & Jahr, 1997: $v_1 = 1 \times 10^6\ \text{M}^{-1}\ \text{s}^{-1}$, $v_2 = 100\ \text{s}^{-1}$, and $v_3 = 20\ \text{s}^{-1}$; density of ~17 800–15 500 μm^{-2} on a disc of 500–1500 nm around the point of release), (○) mark the effect of less efficient transmitter uptake ($v_3 = 300\ \text{s}^{-1}$). Small inset: the decay of particles is approximated by two exponentials (●); $\tau = 0.38$ ms for the fast component and $\tau = 1.7$ ms for the slow component. (——): diffusion model.

inside the cleft, which is comparable to the time course as calculated from the diffusion model*: a decay of transmitter concentration in accordance with experiments (Bartol *et al*., 1994; Clements *et al*. 1992; Spruston *et al*., 1995) is either reproduced in the frame of the kinetic uptake model [eqn (2)] by buffering of transmitter by transporters if a density of ~15 500 to 17 800 μm^{-2} transporters is assumed, or by a net-diffusion coefficient of $D_{net} = 30\ \text{nm}^2\ \mu\text{s}^{-1}$. This indicates a slowing down of transmitter movement by a factor of ~25 compared with free diffusion ($D_{water} = 760\ \text{nm}^2\ \mu\text{s}^{-1}$; Longworth, 1953). Taking into account that the tortuosity of the cleft contributes to slowing down of diffusion by a factor of ~2 to 3 (Garthwaite, 1985; Nicholson & Phillips, 1981; Rise *et al*., 1985; Ichimura & Hashimoto, 1988) we find an estimate of 5170 to 8900 carriers μm^{-2} in the synaptic cleft and its vicinity. Experiments yield a transporter density of 1315 to 13 150 μm^{-2} (Takahashi *et al*., 1996).

Figure 3 (small inset) shows that the time course of transmitter in the cleft can be fitted by a sum of two exponential functions, as assumed by Clements, (1996). In our model the rapid decay ($\tau = 0.38$ ms) arises from the rapid equilibration of molecules across the PSD [see also the fast decrease in the concentration profile in the small inset in Fig. 2(a)] and reflects the fast time-scale of transmitter buffering by transporters (Diamond & Jahr, 1997). The second, lower time constant characterizes the clearance of transmitter from the cleft ($\tau = 1.57$ ms). Variations in the point of release do not contribute essentially (data not shown here), in contrast to differences in the extension of the PSD, which affect the estimate of D_{net} [Fig. 2(b)].

We emphasize that the estimated diffusion coefficient D_{net} is independent of any kinetic receptor model, but is determined by the

*To gain the time course of the total transmitter concentration in the frame of the diffusion model the spatio-temporal concentration profile from eqn (A.2) is integrated over the PSD-area.

parameters R, r_{abs} and $\langle T \rangle$ only. The parameter range is chosen to give an upper limit of the diffusion coefficient D_{net}, which still is about an order of magnitude smaller than the free diffusion coefficient.

2.2. MONTE CARLO SIMULATIONS OF A RECEPTOR POPULATION

Monte Carlo simulations of receptor populations are known to reproduce the experimentally observed noisy character of EPSCs (Korn *et al*., 1993). For a detailed description of the method of Monte Carlo simulations of receptor dynamics we refer to the work of Bartol *et al*. (1991; see also Wahl *et al*., 1996). To model AMPA-/kainate receptors we use the kinetic seven state model (Fig. 4) of Jonas *et al*. (1993). A number of n_{rec} receptors are located at random positions $\mathbf{r}_i$ ($i = 1, \ldots, n_{rec}$), uniformly distributed across the PSD.

In Monte Carlo simulations of receptor populations, we compute individual stochastic trajectories of transmitter molecules instead of the concentration profile of Section A.1. In contrast to most Monte Carlo studies, which treat diffusion on a grid model of the cleft (Agmon & Edelstein, 1997; Bartol *et al*., 1991; Bennett *et al*., 1995, 1997; Faber *et al*., 1992; Kruk *et al*., 1997; Stiles *et al*., 1996) we chose a continuous model of diffusion steps for discrete time steps Δt. The subsequent diffusion steps of single transmitter molecules are then given by a Langevin equation (Gardiner, 1983) for the position $\mathbf{r}_j(t_k) = (x_j(t_k), y_j(t_k))$ of the j-th molecule at time t_k

$$x_n(t_{i+1}) = x_n(t_i) + \eta_1(t_i)\sqrt{2D\Delta t},$$
$$y_n(t_{i+1}) = y_n(t_i) + \eta_2(t_i)\sqrt{2D\Delta t}, \qquad (3)$$

where $\eta_1(t_i)$ and $\eta_2(t_i)$ denote Gaussian distributed random numbers with

$$\langle \eta(t) \rangle = 0; \ \langle \eta_i(t)\eta_j(t') \rangle = \delta_{ij}\delta(t - t').$$

As shown in detail in Bartol *et al*. (1991) statistical averages can either be calculated by averaging over many possible diffusion paths or equivalently by using the spatio-temporal concentration profile $c_\Phi(r, \varphi, t)$, as calculated in Appendix A.1.

For a given distribution of transmitter molecules the receptors are updated in fixed order by calculating the transition probabilities $k_j \Delta t$ for the respective accessible states (see Fig. 4) and comparing it to a random number. Transitions between some of the states of the receptor require the binding of glutamate molecules. In the simplest approximation, this process is modeled by transition rates which depend on the local transmitter concentration. In the seven-state model these are: $\tilde{k}_{+1}$, $\tilde{k}_{+2}$, and $\tilde{k}_{+3}$. To estimate the local transmitter concentration we count the number of molecules inside a disc of "binding-radius" r^j_{bind} around the j-th receptor. The concentration in units of mM is given by dividing this number by the small volume element $\Delta V = h\pi(r^j_{bind})^2$. For instance the transition rate of the j-th receptor to make a transition from $C0$ to $C1$ is computed as

$$\tilde{k}_{+1} = \frac{\begin{pmatrix}\text{no of molecules inside}\\ \text{disc of radius } r^j_{bind}\end{pmatrix} k_{+1}}{(r^{(j)}_{bind})^2 \pi \ h \ N_A},$$

with h denoting the height of the synaptic cleft and N_A Avogadro's number. If a transition into the states $C1$, $C2$ (from $C1$) or $C4$ (from $C3$) occurs, the receptor binds a transmitter molecule, which is being released if the back-transition follows. It should be noted here that the parameter r_{bind} is necessary to determine the local concentration. We checked that the results

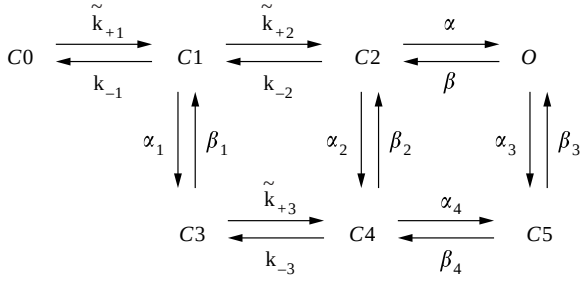

FIG. 4. Kinetic model of an AMPA/kainate-receptor as introduced in Jonas *et al*. (1993). The model differentiates between an open state O, an unbound closed state $C0$, single bound states $C1$ and $C3$ and inactive states $C2$, $C4$, and $C5$. The kinetic rate constants $\tilde{k}_{+i}$, ($i = 1,2,3$) depend on the transmitter concentration, choice of parameters for the rate constants from Jonas *et al*. (1993) set 2.

discussed in Section 3 do not depend on the specific choice of r_{bind}, which was set to 6 nm.

2.3. RECEPTOR DYNAMICS CALCULATED BY CHEMICAL KINETIC EQUATIONS INCLUDING A LOCAL TIME-DEPENDENT CONCENTRATION FIELD

In the following we present a model to calculate post-synaptic EPSCs by chemical kinetic equations, different from the usual approach (Bartol *et al*., 1991; Holmes, 1995; Kleinle *et al*, 1996; Uteshev & Pennefather, 1997): in contrast to other approaches we consider an ensemble of many spatially distributed receptors, each characterized by a set of probabilities to be in one of its accessible states. In addition, each receptor is exposed to a different concentration of glutamate which determines its *individual* transition rates.

Following the work of Land *et al*. (1981, 1984), EPSCs are commonly calculated under the assumption that each receptor in the post-synaptic density "sees" approximately the same glutamate concentration. Then it is sufficient to solve one set of chemical kinetic equations (representing the average over all receptors). The transition rates are determined by the spatially *averaged* glutamate concentration.

We briefly explain our approach. Instead of following the stochastic transitions of n_{rec}, as done in the Monte Carlo simulation, we may alternatively consider the joint probability distribution, to find receptor 1 in state s_1, receptor 2 in state s_2 . . . receptor n in state s_n. This description in terms of probabilities in general involves n_{rec} interacting receptors and is completely equivalent to the stochastic dynamics, as far as averaged quantities are concerned (Gardiner, 1983). Such n particle distribution functions are however difficult to treat analytically or numerically. In our model the interactions among receptors is weak. It is due only to the competition of receptors for neurotransmitter which is abundant at central synapses. If we ignore this interaction, i.e. assume that the number of transmitter molecules temporarily bound to receptors is small compared with the total number, then the distribution for n_{rec} receptors factorizes and we can solve the chemical kinetic equations for each receptor separately. Note however that each receptor i at a given position $\mathbf{r}_i$ "sees" a time-dependent local transmitter concentration $C_i^{(\Delta F)}(t)$ [see eqn (A.4)], which explicitly depends on the position of the receptor and is obtained in Appendix A.3.

As shown in Appendix A.1 the spatio-temporal concentration profile is calculated *analytically*. In the next step we solve the chemical kinetic eqns (A.6) for each receptor i for $i = 1,2, \ldots n_{rec}$. As in the Monte Carlo model we assume that the kinetic rates $\tilde{k}_{+1}^{(i)}$, $\tilde{k}_{+2}^{(i)}$ and $\tilde{k}_{+3}^{(i)}$ of receptor i at position $\mathbf{r}_i$ are proportional to the *local*, time-dependent transmitter-concentration. Hence for every individual receptor i we have to solve a set of seven coupled linear differential equations with time-dependent coefficients given by $C_i^{(\Delta F)}(t)$ in eqn (A.4).

Because the number of receptors is small at central synapses, spatial fluctuations are *not negligible*, giving rise to fluctuations in the EPSCs (see next section). Modelling *individual* receptors in a local time-dependent concentration-field, we treat these fluctuations properly and we are furthermore able to investigate the effects of different spatial arrangements of the receptors on the EPSCs. The only approximation in our model of chemical kinetic equations is the neglect of variations in transmitter concentration due to the binding to and unbinding from post-synaptic receptors. This approximation will be tested by comparison of the results obtained from chemical kinetics to averages over many Monte Carlo runs (see next section). We expect that our assumption is justified for central synapses, where 1000–4000 transmitter molecules interact with 20–100 post-synaptic receptors, in contrast to synapses at the NMJ, where the high number of receptors may affect the transmitter concentration drastically. All other theoretical models, which are used to calculate EPSCs by numerically solving the diffusion equation, employ the same approximation.

2.4. COMPUTATIONAL PROCEDURES

In the Monte Carlo simulation, the concentration profile and the state of all receptors have to be updated simultaneously. For each discrete time step Δt a "new" distribution of transmitter molecules is generated and a possible change in the states of all receptors is calculated. The

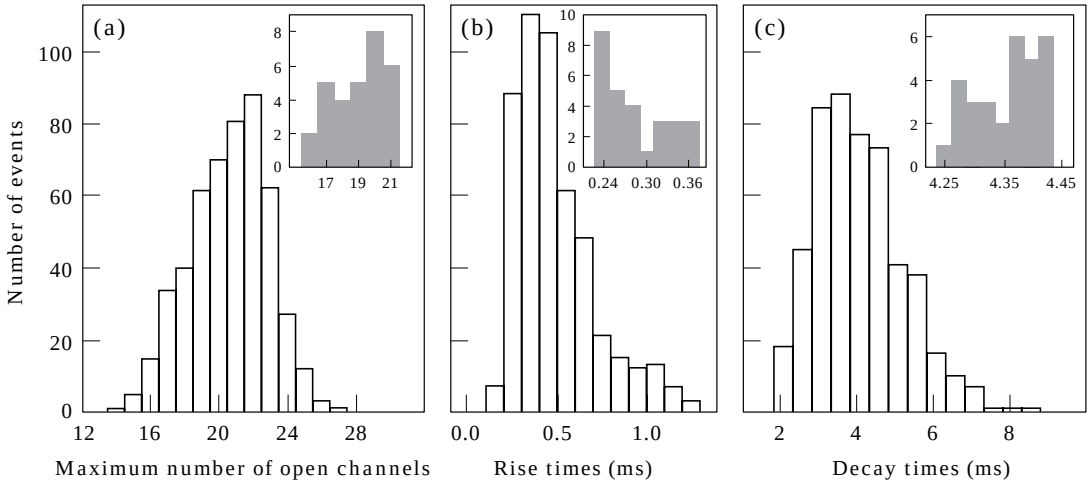

FIG. 5. Distribution of (a) maximum amplitudes, (b) rise times and (c) decay times for 30 randomly distributed receptors on a PSD of $R = 200$ nm, exposed to 3000 transmitter molecules released from a single vesicle in the middle of the synaptic disc ($r_{abs} = 500$ nm, $D_{net} = 30\ \text{nm}^2\ \mu\text{s}^{-1}$). The gray columns in the insets indicate the range of variation due to the spatial distribution of the receptors, calculated from the kinetic model for each receptor position.

choice of Δt explicitly depends on the time-scales of the processes involved: while the diffusion process occurs on a time-scale of μs to ms, the receptor kinetics is much slower (ms to s). For the simulation we choose a time step of 4 μs, which takes the microscopic change in the transmitter concentration into consideration, but still is much faster than the receptor kinetics. We checked (data not shown) that larger and smaller time steps do not alter the results of the simulation.

The computer simulations and numerical routines were written in C language, compiled and run on Pentium PCs. Random numbers were generated using the ran2 routine (Press *et al*., 1992). The coupled set of chemical kinetic equations were solved numerically for discrete time steps using a forth-order Runge Kutta method (Press *et al*., 1992).

3. Results

3.1. STRONGLY FLUCTUATING EPSCS IN ACCORDANCE WITH EXPERIMENTS

We have studied a population of 30 receptors, randomly distributed over the PSD of radius $R = 200$ nm, exposed to 3000 transmitter molecules, which are released from a single vesicle in the center of the PSD. The small value of the diffusion coefficient D_{net} which was estimated in Section 2.1, has been used, and the total number of open channels, i.e. the open probability $P_O^{(tot)}$ as a function of time has been calculated. The signal of a single Monte Carlo run is quite noisy, as shown in Fig. 6(a). To obtain a quantitative measure of the fluctuations we have performed 500 runs and calculated the maximum amplitude, decay and rise time. A histogram of these values is presented in Fig. 5. The distribution of maximum amplitudes has a mean and standard deviation of 20.6 ± 2.3 open channels, corresponding to an open probability of ($\sim$69%), as compared with the experimental value for unitary EPSCs in reduced extracellular Ca^{2+} of $\sim$72% (Jonas *et al*., 1993). For the distribution of rise times (defined as the time elapsed between 20 and 80% of the maximum) we find for mean and standard deviation 0.51 ± 0.26 ms, compared with the experimental values 0.5 ± 0.2 ms of Jonas *et al*. For the distribution of decay times we observe 4.05 ± 1.15 ms compared with 4.1 ± 0.9 ms of Jonas *et al*. (1993). The observed strong fluctuations are in good agreement with experiments and mainly due to the inherent noise in receptor kinetics.

Also displayed is the open probability for a diffusion coefficient which is 10 times larger and often used for theoretical models of transmitter diffusion (see e.g. Busch & Sakmann, 1990; Holmes, 1995; Uteshev & Pennefather, 1997; Wahl *et al*., 1996). It is obvious from Fig. 6(b)

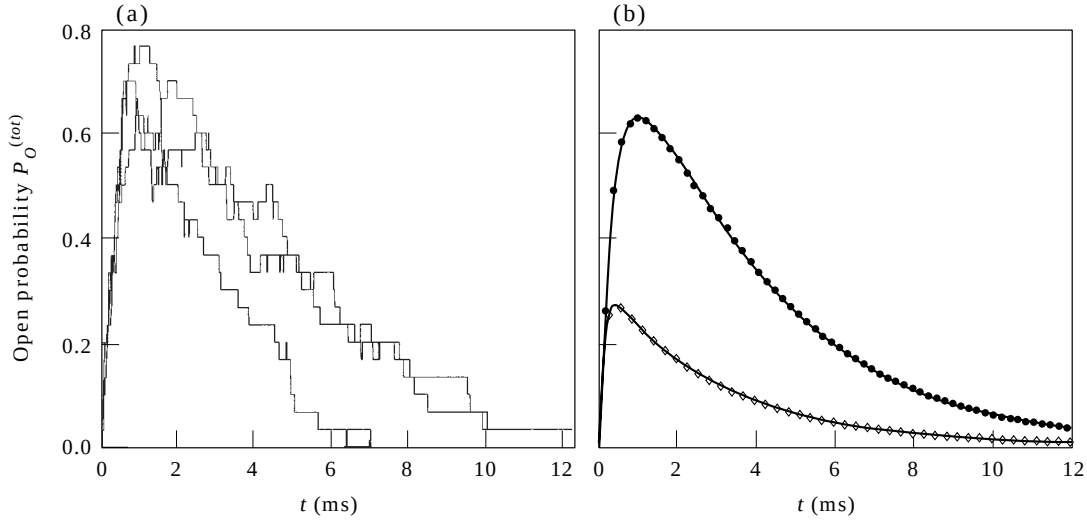

FIG. 6. Open probability $P_O^{(tot)}$ as a function of time (parameters as in Fig. 5). (a) Three examples for the time course of $P_O^{(tot)}$ resulting from a single simulation run; (b) the simulated $P_O^{(tot)}$ (●), averaged over 500 runs, is compared with results from local chemical kinetics (——). Also shown is $P_O^{(tot)}$ as caused by a larger diffusion coefficient of $D_{net} = 300\ \mathrm{nm}^2\ \mu\mathrm{s}^{-1}$ (◇).

that the experimentally determined open probabilities of approximately 60–70% for AMPA/kainate receptors (Hausser & Roth, 1997; Jonas *et al*., 1993; Spruston *et al*., 1995) cannot be reproduced by the commonly used larger value of the diffusion constant D_{net}.

There are several sources of noise, in particular inherent noise in the receptor dynamics and fluctuations due to a spatial distribution of receptors. The Monte Carlo simulation includes both, whereas the noisy receptor dynamics has been averaged out in the kinetic model. This allows us to discriminate between the two noise sources. Within the kinetic model we calculate the open probability for receptors located at a given distance from the site of release, so that we know maximum amplitudes, rise and decay times as a function of distance between receptor and release site. For a given realization of the distribution we can then draw a histogram of maximum amplitudes, rise and decay times, as shown in the inset of Fig. 5 (gray columns). Obviously the *inherent noise* of receptor kinetics is *much stronger* than the fluctuations due to *random distances* between receptors and release site.

3.2. CORRESPONDENCE OF KINETIC AND MONTE CARLO MODEL: BINDING OF TRANSMITTER TO POST-SYNAPTIC RECEPTORS IS NOT A LIMITING FACTOR AT CENTRAL SYNAPSES AND DOES NOT BUFFER TRANSMITTER DIFFUSION

The basic assumption of the kinetic model is that fluctuations of neurotransmitter concentration due to binding and subsequent unbinding of transmitter molecules by post-synaptic receptors can be neglected. To test this assumption, we compare open probabilities $P_O^{(tot)}$ as calculated from the kinetic model with averages over 500 Monte Carlo simulations, using the same amount of released transmitter, the same point of release and the same receptor population. Possible differences in the results are due to transmitter fluctuations because of binding and unbinding. For the same population of 30 receptors the average open probability generated by 500 Monte Carlo runs in Fig. 6(b) is in good correspondence with the result from the kinetic model. Fluctuations due to binding and unbinding of transmitter by receptors can be safely neglected. As displayed in Fig. 7 there is only a very small difference between the open probabilities due to these concentration fluctuations,—

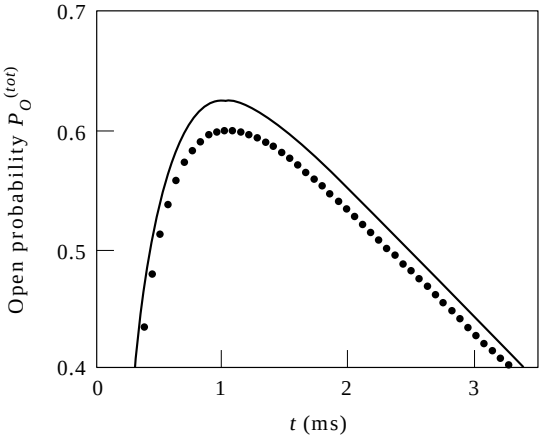

FIG. 7. Difference in the theoretical open probability $P_O^{(tot)}$ between the kinetic model (——), that neglects transmitter binding, and the results of computer simulation (●), $P_O^{(tot)}$ averaged over 500 runs, that include transmitter binding by 300 post-synaptic receptors. Parameters as in Fig. 5.

even if 300 receptors (which exceeds the experimentally estimated number of glutamatergic post-synaptic receptors by far, see e.g. Edmonds *et al*., 1995; Hausser & Roth, 1997; Jonas *et al*., 1993; Spruston *et al*., 1995) compete for transmitter and contribute to transmitter depletion. We therefore conclude that the kinetic model is satisfactory for the calculation of averaged quantities and subsequently will use it to study systematic effects of different receptor distributions.

Furthermore the agreement of the kinetic model and the Monte Carlo simulations shows that buffering of transmitter by binding to post-synaptic receptors is a very small effect compared with the influence of transporter–transmitter interaction on the transmitter dynamics (Section 2.1): the number of post-synaptic receptors (30 to 100) is too small to noticeably affect the motion of 1000 to 5000 transmitter molecules.

3.3. EFFECTS OF DIFFERENT RECEPTOR ARRANGEMENTS

The model is used to study the effect of *different spatial arrangements* of receptors on the post-synaptic side. Changes of the synaptic geometry from simple to perforated (clustered) synapses have been suggested as a possible mechanism of LTP (Edwards, 1995a). We compare EPSCs of a simple synapse with an unperforated PSD (Fig. 8) with a perforated synapse as shown in Fig. 9. Each cluster of the perforated PSD is associated with a possible release site of pre-synaptic vesicles and contains the same number of receptors as distributed across the simple PSD (30 receptors). First, the simulation is used to visualize the effects of transmitter diffusion on the receptor dynamics. Four snapshots of 30 randomly distributed receptors on a PSD of 200 nm radius at different times after the release of a single vesicle are shown in Fig. 8. One observes how the opening of channels coincides with the spreading of transmitter. Following the release of a single vesicle containing 3000 molecules 60% of the receptors are in one of the inactive states $C3$, $C4$, or $C5$ after the transmitter has been cleared from the cleft. Figure 10(a) indicates that the simple synapse is saturated to $\sim 70\%$ by the release of a single vesicle and saturated after the simultaneous release of two vesicles (as discussed in e.g. Busch & Sakmann, 1990; Edwards, 1991; Bennett *et al*., 1997), while in contrast the amplitude distribution at perforated synapses [Fig. 10(b)] does not exhibit saturation after the release of two vesicles. The distribution of rise times becomes narrower and shifts towards faster rise times (Fig. 11) as more vesicles are released. At the perforated PSD the change in the distribution of rise times [Fig. 11(b)] is stronger than for the simple synapse [Fig. 11(a)], since the broadening of the rise time distribution for the release of one vesicle is caused by the late activation of receptors from distant clusters. Distributions of decay times do not change systematically with the amount and position of transmitter released (data not shown) and are mostly determined by the stochasticity of the individual receptor dynamics.

3.4. POST-SYNAPTIC MECHANISMS FOR SYNAPTIC POTENTIATION

Synaptic plasticity is often discussed in the context of quantal analysis, where it is assumed that each vesicle encounters the same distribution of post-synaptic receptors. If this assumption holds, then the "quantum" of transmitter defined as the content of one vesicle, is actually transferred as a whole to the post-synaptic side, so that the post-synaptic

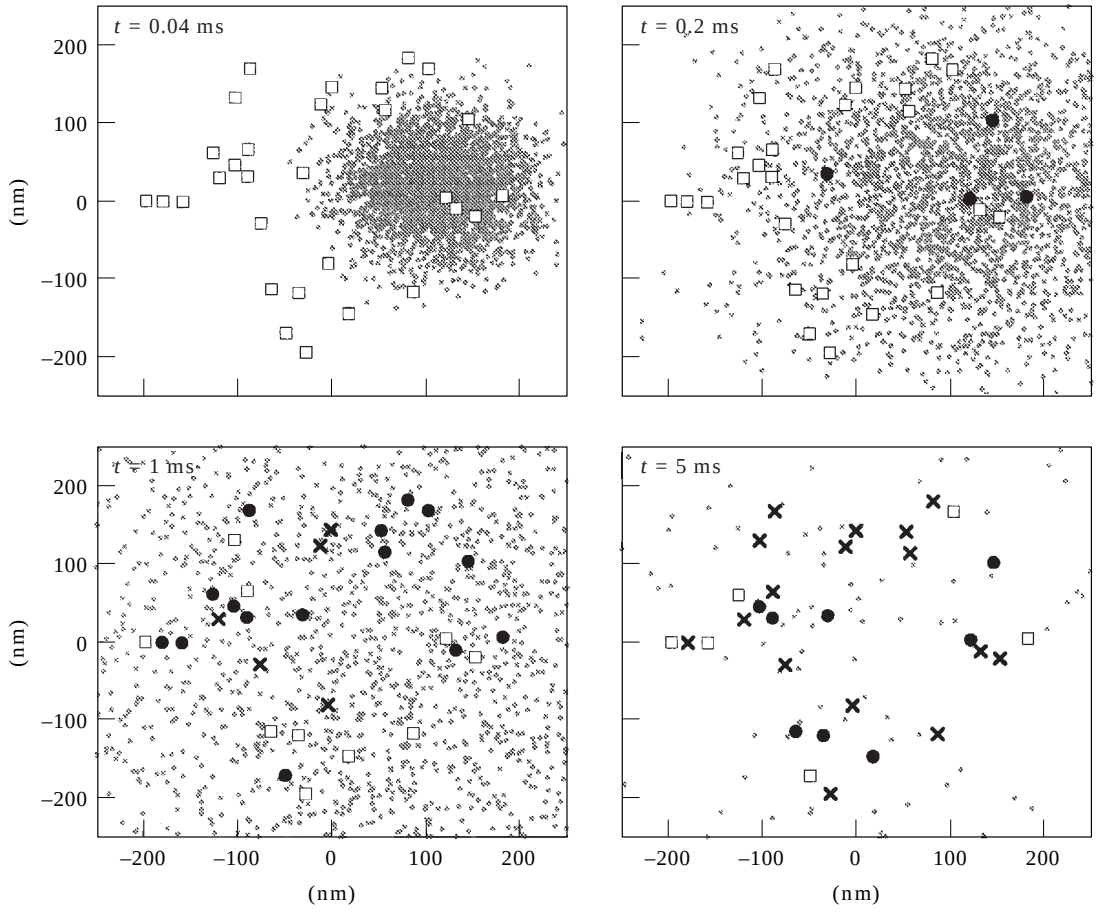

FIG. 8. Receptor distribution on a simple synapse; states of 30 randomly distributed receptors at times $t = 0.04$, 0.2, 1, and 5 ms after release of a single vesicle (at a randomly chosen release site within the PSD), which contains 3000 molecules (small gray circles); rest of parameters as in Fig. 5. At time $t = 0$ all the receptors are in the closed unbound state $C0$ (□, inactive states $C1$ and $C2$ also displayed as □), but start to open (state O, ●) or desensitize (inactive states $C3$, $C4$, and $C5$, ×).

current is approximately quantized according to the number of released vesicles (for a review see, e.g. McLachlan, 1978). As seen in the previous paragraph the PSD is partially saturated by one vesicle and only a gradual increase in post-synaptic current is observed, if more than one vesicle per bouton is released. Hence standard quantal analysis does not apply. In the extreme case of complete saturation by one vesicle, one might again expect to observe multiple quanta due to several boutons. However the quanta are then determined by the mean number of receptors in the PSD of one bouton (see e.g. Bekkers, 1994; Redman, 1990) and the transition rates of the single channel, suggesting a post-synaptic mechanism for potentiation*. In the case of strong saturation, changes in vesicle content or changes in the incidence of multi-vesicular release will hardly change the post-synaptic current and hence cannot serve as mechanisms for potentiation.

In the following we discuss mechanisms of synaptic potentiation which are located on the post-synaptic side. We first investigate rather smooth changes in the distribution of receptors, e.g. the size or the shape of the PSD is varied, while the total number of receptors is kept constant, as suggested as a first step of change in synaptic structure by Edwards (1995a). A possible arrangement of receptors on the

*We do not discuss here an overall increase in release probability, resulting in an activation of silent synaptic boutons.

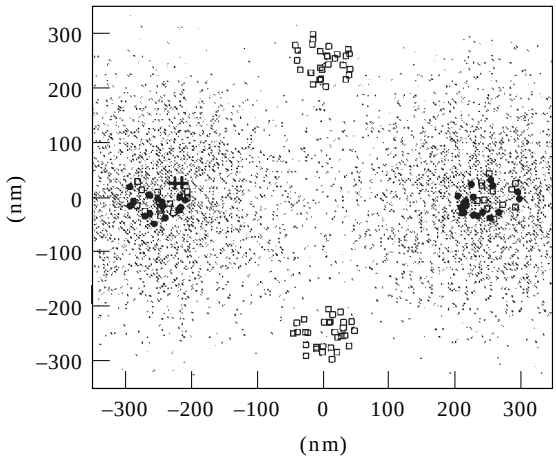

FIG. 9. States of 120 receptors distributed in four clusters, each with a diameter of 100 nm at time $t = 0.2$ ms. Two vesicles have been released at time $t = 0$ in the center of two clusters, each vesicle containing 3000 molecules; rest of parameters as in Fig. 8.

post-synaptic membrane located near the point of transmitter release (here in the middle of the synaptic disc) is shown in Fig. 12(a). The same number of receptors have been distributed according to a Gaussian distribution, where the standard deviation σ characterizes the average distance of the receptors from the point of release. For smaller values of σ the receptors are clustered closer to the point of release, while for higher values of σ the receptor distribution resembles a random homogeneous receptor distribution. The calculated open probability $P_O^{(tot)}$ in Fig. 12(b) reveals that a clustering of post-synaptic receptors causes a relatively weak potentiation of the peak amplitude, e.g. a 15 to 20% change for $\sigma = 50$ and 100 nm. This is to be expected, because of the abundance of neurotransmitter molecules and the fact that the transmitter concentration equilibrates within a few hundred μs (small inset in Fig. 2), which is fast compared with the receptor kinetics*. To double the open probability, keeping the total number of receptors fixed, requires a 64 times smaller active zone. Such extreme changes seem to be more realistic in the context of structural changes of synaptic morphology.

*Again the explicit choice of ΔF proved not to be crucial for the calculated results (data not shown).

A much more effective potentiation is achieved by increasing the number of post-synaptic receptors. We find that the maximum amplitudes of EPSCs are directly proportional to the total number of receptors [Fig. 13(a)]. The normalized open probability for the same PSD with 30, 80 and 150 receptors is compared in Fig. 13(b). The differences between the two curves are very small (and due to transmitter depletion because of binding to post-synaptic receptors) and hence the EPSCs increase to a very good approximation *linearly* with the total number of receptors.

The number of receptors can be increased in at least two qualitatively different ways. Either

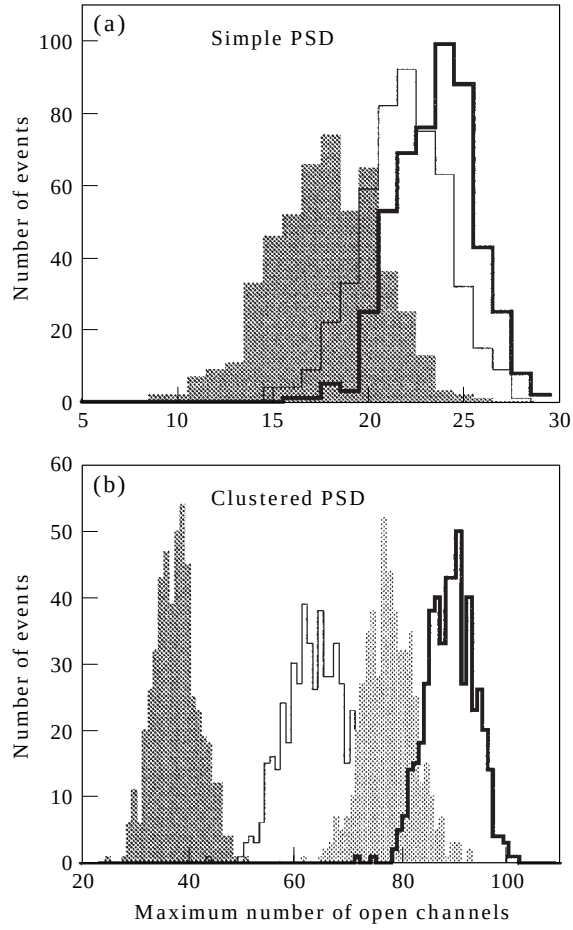

FIG. 10. Effect of multiple release on the distribution of maximum amplitudes of (a) 30 receptors distributed randomly across a simple PSD (Fig. 8) and (b) 120 receptors distributed in four receptor clusters of 30 receptors each (Fig. 9). Amplitude distribution for one (dark gray columns), two (solid line), three (light gray columns) and four (thick solid line) vesicles released, generated from 500 simulation runs (parameters as in Figs 8 and 9).

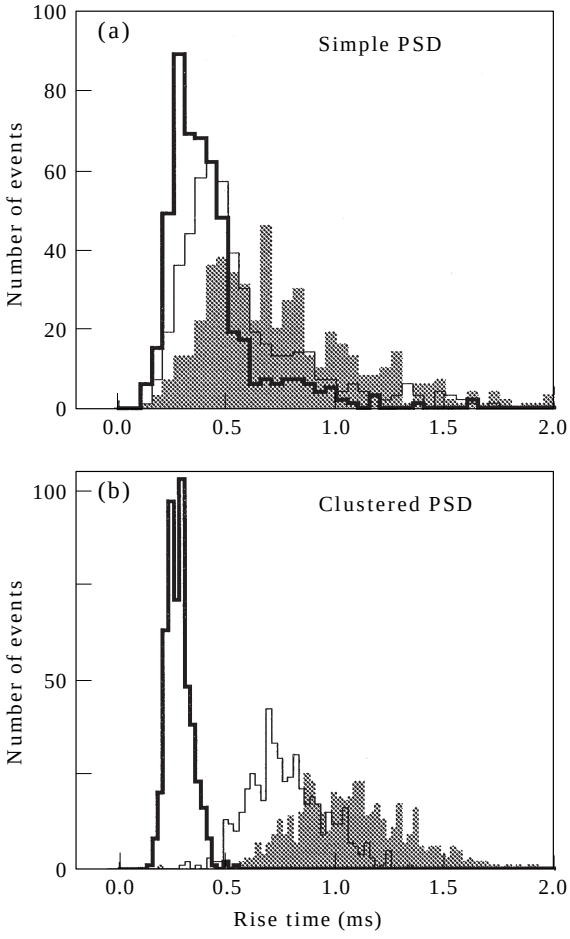

FIG. 11. Effect of multiple release on the distribution of rise times of (a) 30 receptors distributed randomly across a simple PSD (Fig. 8) and (b) 120 receptors distributed in four receptor clusters of 30 receptors each (Fig. 9). Distribution of rise times for one (dark gray columns), two (solid line), and four (thick solid line) vesicles released, generated from 500 simulation runs (parameters as in Figs 8 and 9).

the geometry of the synapse is left unchanged or alternatively new boutons are created. (Another possibility may be the activation of silent synapses). Edwards (1995a) has suggested perforation of a simple synapse into several clusters of receptors, where the different receptor clusters act as nearly independent release sites, together with an overall increase in the number of receptors, as an effective mechanism for potentiation. Following this idea multiple release at perforated synapses could account for a skew in amplitude distributions of miniature currents (for a detailed discussion see Edwards, 1995b). We follow this suggestion and assume four possible release sites: at the simple synapse they are randomly distributed across the PSD as in Fig. 8, while at the perforated synapse each release site is associated with a receptor cluster (Fig. 9). The probability p for release of a vesicle is assumed to be the same for all four release sites. As displayed in Fig. 14 the shape of the amplitude distribution varies with a change in the release probability p from 0.05 to 0.4 from a non-skewed to a skewed distribution for the perforated synapse, while the distribution for the simple synapse does not seem to change systematically. For higher release probabilities the skew again vanishes or even appears towards smaller amplitudes. A detailed study and

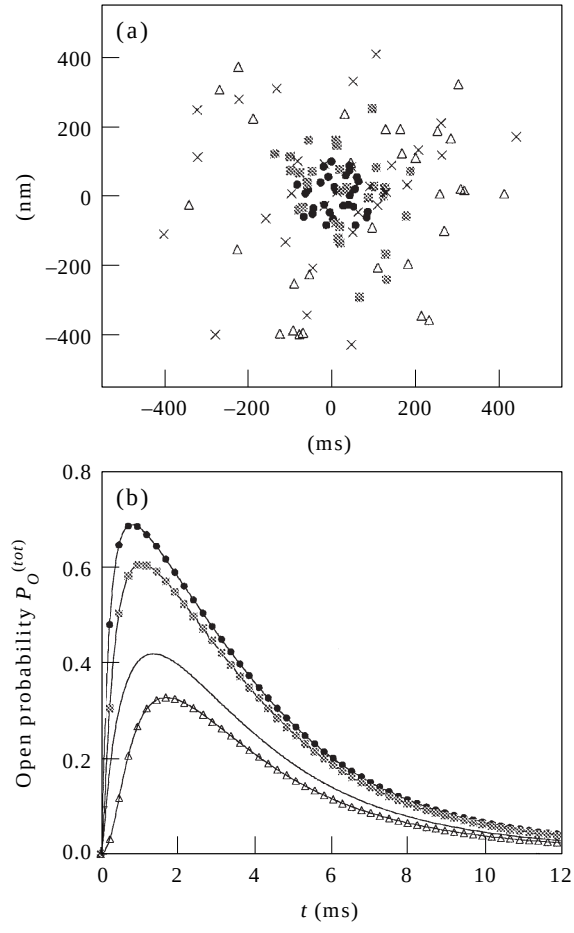

FIG. 12. (a) 30 receptors distributed according to a Gaussian distribution centered around the point of release (= middle of synaptic disc). Here σ denotes the standard deviation of the Gaussian; (b) total open probability $P_O^{(tot)}$ as function of time for the receptor distributions in (a), as calculated from the kinetic model; rest of parameters as in Fig. 5, $\sigma = 50$ (●), 100 (▩), 200 (×, ——) and 400 nm (△).

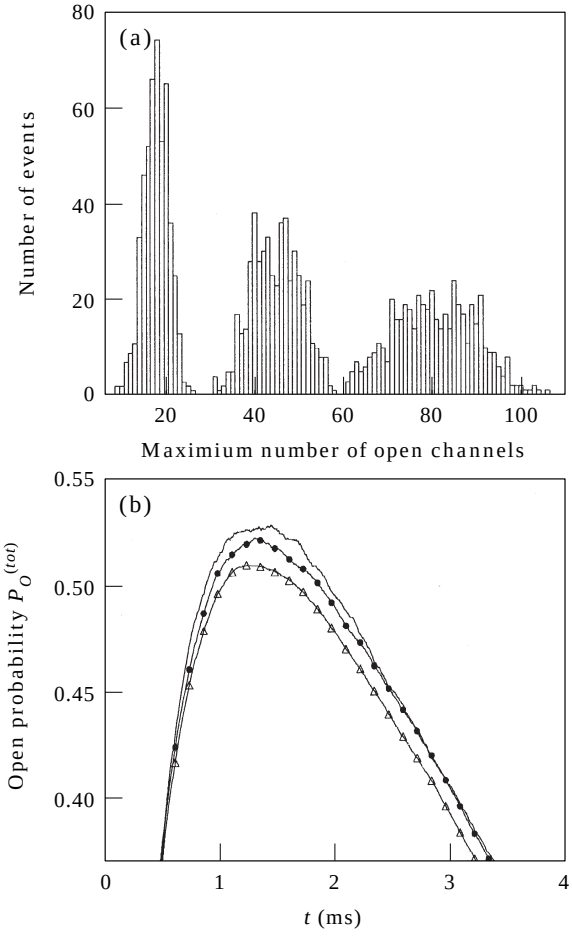

FIG. 13. (a) Distributions of amplitudes for 30, 80 and 150 receptors distributed randomly on a PSD of fixed size ($R = 200$ nm) for a random point of release, generated from 500 runs, rest of parameters as in Fig. 5; (b) corresponding open probabilities $P_O^{(tot)}$, averaged over 500 runs, for 30 (——), 80 (●) and 150 receptors (△).

discussion will follow in a second paper and has been published in preliminary form (Trommershäuser *et al*., 1997).

4. Conclusion

In this paper we have discussed a theoretical model of synaptic transmission, derived from experimental data on single channel kinetics, transmitter–transporter interactions and the mean residence time of glutamate in the cleft. On the one hand we have used Monte Carlo simulations, which have been introduced by Bartol *et al*. (1991) for synapses at the NMJ, and transfered the approach to transmission processes at central synapses. On the other hand we have derived a simplified model in terms of *local* chemical kinetic equations, i.e. each receptor is characterized by a set of probabilities to be in any one of its accessible states. This simplified model relies heavily on the fact that at central synapses the transmitter molecules of a single vesicle provide an abundance of neurotransmitter for a low number of post-synaptic receptors. In other words the local chemical kinetics would not work at the NMJ and has been designed specifically for synapses in the CNS.

It was our intention to keep the number of free model parameters as low as possible and the fitting to experiments as transparent as possible. We have proposed a simple description of the synaptic cleft as a flat disc with finite lateral extension. Transmitter molecules are allowed to diffuse up to a maximum distance, which is identified with the typical distance to neighboring synapses and which is modeled theoretically as an absorbing boundary. This approach allows us to estimate the net-diffusion coefficient D_{net} of transmitter inside the cleft on the basis of *experimentally known* parameters only. We find $D_{net} \sim 20$–$50\ \mathrm{nm^2\,\mu s^{-1}}$ for glutamate inside the cleft, implying a strong reduction as compared with free diffusion in aqueous solution. Possible explanations are the tortuosity of the cleft and interactions with transporter molecules, distributed with a density of 5170 to 8900 transporters $\mu\mathrm{m}^{-2}$ in the synaptic cleft and its vicinity.

We have used the complementary theoretical approaches of Monte Carlo simulations and local chemical kinetics to calculate EPSCs. This enables us to compare the two approaches in detail and show their equivalence for average currents. The noisy character of the EPSCs is apparent in broad distributions of amplitudes, rise and decay times of individual EPSCs in good agreement with experiments (Jonas *et al*., 1993). We have shown that the fluctuations are mainly due to the inherent noise in the receptor dynamics, whereas spatial fluctuations are less important. We conclude that despite the simplicity of our model it seems to comprise the relevant features of the transmission process to reproduce experimental data for average currents as well as the statistical properties of EPSCs.

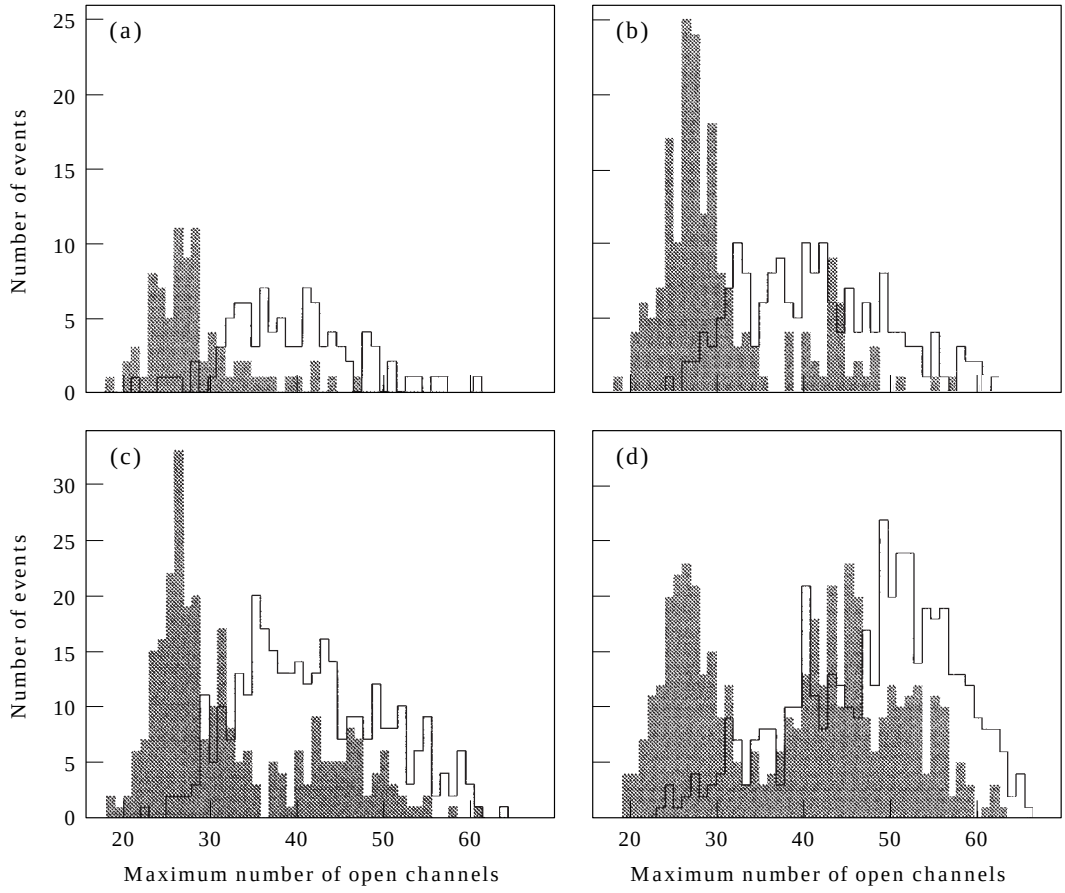

FIG. 14. Distributions of peak amplitudes (maximum number of open channels), each distribution generated for 120 receptors from 500 runs. Different panels show distributions for varying release probabilities: (a) $p = 0.05$/failure rate $\sim 80\%$, (b) $p = 0.1$/failure rate $\sim 66\%$, (c) $p = 0.2$/failure rate $\sim 41\%$ and (d) $p = 0.4$/failure rate $\sim 12\%$ (d). The gray distributions are from perforated synapses (parameters as in Fig. 9). The corresponding white distributions result from the release of four vesicles at random release sites across the PSD at a simple synapse with 120 receptors (rest of parameters as in Fig. 5). The failure rates denote the percentage of events without the release of any vesicle. (Grey columns) clustered PSD; (white columns) simple PSD.

Subsequently we have used the model to study different receptor distributions as well as post-synaptic mechanisms for potentiation. Changes in the receptor distribution, e.g. clustering of receptors, do not efficiently potentiate post-synaptic signals, as long as the total number of receptors stays the same. An increase in the number of post-synaptic receptors or a change of receptor kinetics as e.g. discussed in Ambros-Ingerson & Lynch, (1993) and Marienhagen *et al*. (1997) are found to be much more effective for potentiation.

Our future work will discuss potentiation of post-synaptic currents due to the activation of silent synaptic boutons by an overall increased probability of vesicle release or potentiation due to forming perforated synapses with multiple release sites (see Edwards, 1995a). Possible mechanisms shaping miniature amplitude distributions as outlined in the last paragraph will be studied in this context.

We gratefully acknowledge stimulating discussion with Frances A. Edwards and Hemai Parthasarathy, David Colquhoun, Reiner Kree, and Kamal Bhattacharya. This work has been supported by the DFG through Graduiertenkolleg *Organisation und Dynamik neuronaler Netzwerke*.

REFERENCES

AGMON, N. & EDELSTEIN, A. L. (1997). Collective binding properties of receptor arrays. *Biophys. J.* **72,** 1582–1594.
AMBROS-INGERSON, J. & LYNCH, G. (1993). Channel gating kinetics and synaptic efficacy: a hypothesis for expression

of long-term potentiation. *Proc. Nat. Acad. Sci. U.S.A.* **90,** 7903–7907.

Asztely, F., Erdemli, G. & Kullmann, D. M. (1997). Extrasynaptic glutamate spillover in the hippocampus: dependence on temperature and the role of active glutamate uptake. *Neuron* **18,** 281–293.

Barbour, B., Keller, B. U., Llano, I. & Marty, A. (1994). Prolonged presence of glutamate during excitatory synaptic transmission to cerebellar Purkinje cells. *Neuron* **12,** 1331–1343.

Bartol, T. M., Land, B. R., Salpeter, E. E. & Salpeter, M. M. (1991). Monte Carlo simulation of miniature endplate current generation in the vertebrate neuromuscular junction. *Biophys. J.* **59,** 1290–1307.

Bekkers, J. M. (1994). Quantal analysis of synaptic transmission in the central nervous system. *Curr. Opin. Neurobiol.* **4,** 360–365.

Bennett, M. R., Farnell, L., Gibson, W. G. & Karunanithi, S. (1995). Quantal transmission at purinergic junctions: stochastic interaction between ATP and its receptors. *Biophys. J.* **68,** 925–935.

Bennett, M. R., Farnell, L., Gibson, W. G. & Lavidis, N. A. (1997). Synaptic transmission at visualized sympathetic boutons: stochastic interaction between acetylcholine and its receptors. *Biophys. J.* **72,** 1595–1606.

Bergles, D. E. & Jahr, C. E. (1997). Synaptic activation of glutamate transporters in hippocampal astrocytes. *Neuron.* **19,** 1297–1308.

Busch, C. & Sakmann, B. (1990). Synaptic transmission in hippocampal neurons. Numerical reconstruction of quantal IPSCs. *Cold Spring Harbor Symp. Quant. Biol.* **LV,** 69–80.

Clements, J. D. (1996). Transmitter time course in the synaptic cleft: its role in central synaptic function. *Trends Neurosci.* **19,** 163–171.

Clements, J. D., Lester, R. A. J., Tong, G., Jahr, C. E. & Westbrook, G. L. (1992). The time course of glutamate in the synaptic cleft. *Science* **258,** 1498–1501.

Colquhoun, D. & Hawkes, A. G. (1995). The principles of the stochastic interpretation of ion-channel mechanisms. In: *Single-Channel Recording* (Sakmann, B. & Neher, E., eds) 2nd Edn, pp. 397–481. New York: Plenum Press.

Diamond, J. &Jahr, C. (1997). Transporters buffer synaptically released glutamate on a submillisecond time scale. *J. Neurosc.* **17,** 4672–4687.

Edmonds, B., Gibbs, A. J. & Colquhoun, D. (1995). Mechanisms of activation of glutamate receptors and the time course of excitatory synaptic currents. *Annu. Rev. Physiol.* **57,** 495–519.

Edwards, F. A. (1991). LTP is a long term problem. *Nature* **350,** 271–272.

Edwards, F. A. (1995a). LTP—a structural model to explain the inconsistencies. *Trends Neurosci.* **18,** 250–255.

Edwards, F. A. (1995b). Anatomy and electrophysiology of fast central synapses lead to a structural model for long-term potentiation. *Physiol. Rew.* **75,** 759–787.

Faber, D. S., Young, W. S., Legendre, P. & Korn, H. (1992). Intrinsic quantal variability due to stochastic properties of receptor–transmitter interactions. *Science* **258,** 1494–1498.

Gardiner, C. W. (1983). *Handbook of Stochastic Methods.* Berlin: Springer.

Garthwaite, J. (1985). Cellular uptake disguises action of L-glutamate on N-methyl-D-aspartate receptors. *Br. J. Pharmacol.* **85,** 297–307.

Harris, K. M. & Kater, S. B. (1994). Dendritic spines: cellular specializations imparting both stability and flexibility to synaptic function. *Annu. Rev. Neurosci.* **17,** 341–371.

Hausser, M. & Roth, A. (1997). Dendritic and somatic glutamate receptor channels in rat cerebellar Purkinje cells. *J. Physiol.* (*Lond.*) **501,** 77–95.

Hertz, L., Schousboe, A, Boechler, N., Mukerji, S. & Fedoroff, S. (1978). Kinetic characteristics of the glutamate uptake into normal astrocytes in cultures. *Neurochem. Res.* **3,** 1–14.

Holmes, W. R. (1995). Modeling the effect of glutamate diffusion and uptake on NMDA and non-NMDA receptor saturation. *Biophys. J.* **69,** 1734–1747.

Ichimura, T. & Hashimoto, P. H. (1988). Structural components in the synaptic cleft captured by freeze-substitution and deep etching of directly frozen cerebellar cortex. *J. Neurocytol.* **17,** 3–12.

Isaacson, J. S. & Nicoll, R. A. (1993). The uptake inhibitor L-trans-PDC enhances responses to glutamate but fails to alter the kinetics of excitatory synaptic currents in the hippocampus. *J. Neurophysiol.* **70,** 2187–2191.

Jonas, P., Major, G. & Sakmann, B. (1993). Quantal components of unitary EPSCs at the mossy fiber synapse on CA3 pyramidal cells of rat hippocampus. *J. Physiol.* (*Lond.*) **472,** 615–663.

Khanin, R., Parnas, H. & Segel, L. (1994). Diffusion cannot govern the discharge of neurotransmitter in fast synapses. *Biophys. J.* **67,** 966–972.

Kleinle, J., Vogt, K., Luescher, H. R., Mueller, L., Senn, W., Wyler, K. & Streit, J. (1996). Transmitter concentration profiles in the synaptic cleft: analytical model of release and diffusion. *Biophys. J.* **71,** 2413–2426.

Korn, H., Bausela, F., Charpier, S. & Faber, D. S. (1993). Synaptic noise and multiquantal release at dendritic synapses. *J. Neurophysiol.* **70,** 1249–1254.

Kruk, P. J., Korn, H. & Faber, D. S. (1997). The effect of geometrical parameters on synaptic transmission: a Monte Carlo simulation study. *Biophys. J.* **73,** 2874–2890.

Kullmann, D. A. & Asztely, F. (1998). Extrasynaptic glutamate spillover in the hippocampus: evidence and implications. *Trends Neurosci.* **21,** 8–14.

Land, B. R., Salpeter, E. E. & Salpeter, M. M. (1981). Kinetic parameters for acetylcholine interaction in intact neuromuscular junction. *Proc. Nat. Acad. Sci. U.S.A.* **78,** 7200–7204.

Land, B. R., Harris, W. V., Salpeter, E. E. & Salpeter, M. M. (1984). Diffusion and binding constants for acetylcholine derived from the falling phase of miniature endplate currents. *Proc. Nat. Adac. Sci. U.S.A.* **81,** 1594–1598.

Longworth, L. G. (1953). Diffusion measurement at 25°, of aqueous solutions of amino acids, peptides and sugars. *J. Am. Chem. Soc.* **75,** 5705–5709.

McLachlan, E. M. (1978). The statistics of transmitter release at chemical synapses. *Int. Rev. Physiol.* **17,** 49–117.

Marienhagen, J. & Zippelius, A. (1995). Monte Carlo simulation of a structural model for long-term potentiation. In: *Supercomputing in Brain Research* (Hermann, H. J., Wolf, D. E. & Poeppel, E., eds). Singapore: World Scientific.

Marienhagen, J., Keller, B. U. & Zippelius, A. (1997). Kinetic model of excitatory synaptic transmission to cerebellar Purkinje cells. *J. theor. Biol.* **188,** 227–240.

MENNERICK, S., DHOND, R. P., BENZ, A., XU, W., ROTHSTEIN, J. D., DANBOLT, N. C., ISENBERG, K. E. & ZORUMSKI, C. F. (1998). Neuronal expression of the glutamate transporter GLT-1 in hippocampal microcultures. *J. Neurosc.* **18,** 4490–4499.

NICHOLSON, C. & PHILLIPS, J. M. (1981). Ion diffusion modified by tortuosity and volume fraction in the extracellular microenvironmet of the rat cerebellum. *J. Physiol.* (*Lond.*) **321,** 225–257.

OTIS, T. S., KAVANAUGH, M. P. & JAHR, C. (1997). Postsynaptic glutamate transport at the climbing fiber-Purkinje cell synapse. *Science* **277,** 1515–1518.

PETERS, A. & KAISERMAN-ABRAMOF, I. R. (1969). The small pyramidal neuron of the rat cerebral cortex: the synapses upon dendritic spines. *Zeitsch. Zellforsch.* **100,** 487–506.

PRESS, W. P., TEUKOLSKY, S. A., VETTERLING, W. T. & FLANNERY, B. P. (1992). *Numerical Recipes in C. The Art of Scientific Computing* 2nd Edn. Cambridge: Cambridge University Press.

REDMAN, S. J. (1990). Quantal analysis of synaptic potentials in neurons of the central nervous system. *Physiol. Rev.* **70,** 165–198.

RISE, M. E., GERHARDT, G. A., HIERL, P. M., NAGY, G. & ADAMS, R. N. (1985). Diffusion coefficients of neurotransmitters and their metabolites in brain extracellular fluid space *Neuroscience* **3,** 891–902.

RUSAKOV, D. A. & KULLMANN, D. M. (1998). Extrasynaptic glutamate diffusion in the hippocampus: ultrastructural constraints, uptake, and receptor activation. *J. Neurosci.* **18,** 3158–3170.

SPRUSTON, N., JONAS, P. & SAKMANN, B. (1995). Dendritic glutamate receptor channels in rat hippocampal CA3 and CA1 pyramidal neurons. *J. Physiol.* **482,** 325–352.

STILES, J. R., VAN HELDEN, D., BARTOL, T. M., SALPETER, E. D. & SALPETER, M. M. (1996). Miniature endplate current rise time < 100 ms from improved dual recordings can be modeled with passive acetylcholine diffusion from a synaptic vesicle. *Proc. Nat. Acad. Sci. U.S.A.* **93,** 5747–5752.

TAKAHASHI, M., SARANTIS, M. & ATWELL, D. (1996). Postsynaptic glutamate uptake in rat cerebellar Purkinje cells. *J. Physiol.* **497,** 525–530.

TONG, G. & JAHR, C. E. (1994). Multivesicular release from excitatory synapses of cultured hippocampal neurons. *Neuron* **12,** 51–59.

TONG, G. & JAHR, C. E. (1994). Block of glutamate transporters potentiates postsynaptic excitation. *Neuron* **13,** 1195–1203.

TROMMERSHAEUSER, J., PARTHASARATHY, H., EDWARDS, F. A. & ZIPPELIUS, A. (1997). Stochastic models of the synaptic transmission in the CNS: importance of the diffusion coefficient and the receptor distribution. *Soc. Neurosci. Abs.* **23,** 658.

UTESHEV, V. V. & PENNEFATHER, P. S. (1996). A mathematical description of MPSC generation at CNS synapses. *Biophys. J.* **71,** 1256–1266.

UTESHEV, V. V. & PENNEFATHER, P. S. (1997). Analytical description of the activation of multi-state receptors by continuous neurotransmitter signals at brain synapses. *Biophys. J.* **72,** 1127–1134.

VAN DEN LOOS, H. (1963). Fine structure of synapses in the cerebral cortex. *Zeitsch. Zellforsch.* **60,** 815–825.

WADICHE, J. I., ARRIZA, J. L., AMARA, S. G. & KAVANAUGH, M. (1995). Kinetics of a human glutamate transporter. *Neuron* **14,** 1019–1027.

WAHL, L.M., POUZAT, C. & STRATFORD, K. J. (1996). Monte Carlo simulation of fast excitatory synaptic transmission at a hippocampal synapse. *J. Neurophysiol.* **75,** 597–608.

WANG, G. J., CHUNG, H. J., SCHNUER, J., PRATT, K., ZABLE, A. C., KAVANAUGH, M. P. & ROSENBERG, P. A. (1998). High affinity glutamate transport in rat cortical neurons in culture. *Mol. Pharmacol.* **53,** 88–96.

APPENDIX

A.1. Computation of the Diffusive Concentration Profile

The spatio-temporal concentration profile $c(r,\varphi,z,t)$ of a number of N_T transmitter molecules in the cleft is calculated by solving the three-dimensional diffusion equation

$$\frac{\partial}{\partial t}\,\mathrm{c(r,\varphi,z,t)} = N_T D_{net}\left[\frac{\partial^2}{\partial r^2}+\frac{1}{r}\frac{\partial}{\partial r}+\frac{1}{r^2}\frac{\partial^2}{\partial \varphi^2}+\frac{\partial^2}{\partial z^2}\right]c(r,\varphi,z,t), \tag{A.1}$$

Since the synaptic cleft is chosen as a flat cylinder of height h and radius R cylindrical coordinates z,r,φ are used. The solution of the diffusion eqn (A.1) is unique, provided we specify initial and boundary conditions. We assume that all molecules start at $t = t_0$ from a point at position $\mathbf{r}_0$, i.e.

$$c(\mathbf{r},t=0) = \frac{N_T}{r}\,\delta(r-r_0)\delta(\varphi-\varphi_0)\delta(z-h).$$

Diffusing molecules which reach the absorbing boundary at r_{abs} are taken out of the system. Transmitter molecules cannot escape in the z-direction, corresponding to a reflecting boundary at $z = 0$ and $z = h$. These boundary conditions are summarized by the equations:

(a) reflecting boundary at

$$z = 0,\ z = h\text{: } \frac{\partial}{\partial z}c(\mathbf{r},t)\bigg|_{z=0} = \frac{\partial}{\partial z}c(\mathbf{r},t)\bigg|_{z=h} = 0$$

(b) absorbing boundary at

$$r = r_{abs}\text{: } \mathrm{c}(\mathbf{r},t)|_{r=r_{abs}} = 0.$$

Because of the specific form of boundary and initial conditions the solution of eqn (A.1) separates into a one-dimensional probability distribution $p_z(z,t)$ to account for the distribution of molecules in the z-direction and into a

two-dimensional "lateral" probability distribution $p_\Phi(r,\varphi,t)$

$$c(\mathbf{r},t) = N_T p_\Phi(r,\varphi,t) p_z(z,t),$$

with

$$p_z(z,t) = \sum_{n=-\infty}^{+\infty} \frac{(-1)^n}{h} \cos\left(\frac{n\pi z}{h}\right) \mathrm{e}^{-\frac{n^2\pi^2}{h^2} D_{net} t},$$

$$p_\Phi(r,\varphi,t) = -\frac{1}{r_{abs}^2 \pi}\left[\sum_{m=0}^{\infty}\sum_{n=1}^{\infty} \frac{J_m(\alpha_{mn} r_0)}{J_{m-1}(\lambda_{mn}) J_{m+1}(\lambda_{mn})} J_m(\alpha_{mn} r)\, \mathrm{e}^{-\alpha_{mn}^2 D_{net} t} \right.$$

$$\left.\left\{[1+(-1)^m]\cos(m\varphi_0)\cos(m\varphi) + [1-(-1)^m]\sin(m\varphi_0)\sin(m\varphi)\right\}\right]. \quad \text{(A.2)}$$

Here J_m denotes the m-th Bessel function of the first kind, λ_{mn} the n-th zero of J_m and $\alpha_{mn} = \lambda_{mn}/r_{abs}$.

The mean residence time of transmitter in the cleft $\langle T \rangle$ is calculated by integrating the two-dimensional concentration profile p_Φ in eqn (A.2) over the area of the PSD and all times, i.e.

$$\langle T \rangle = \int_0^\infty \mathrm{d}t \int_0^{2\pi} \mathrm{d}\varphi \int_0^R \mathrm{d}r\; r\; p_\Phi(r,\varphi,t)$$

$$= -\frac{1}{r_{abs}^2 \pi} \sum_{m=0}^{\infty}\sum_{n=1}^{\infty} \int_0^\infty \mathrm{d}t\, \mathrm{e}^{-\alpha_{mn}^2 D_{net} t} \int_0^R \mathrm{d}r\; r\; \frac{J_m(\alpha_{mn} r_0)}{J_{m-1}(\lambda_{mn}) J_{m+1}(\lambda_{mn})} J_m(\alpha_{mn} r)$$

$$\underbrace{\int_0^{2\pi} \mathrm{d}\varphi \left\{[1+(-1)^m]\cos(m\varphi_0)\cos(m\varphi) + [1-(-1)^m]\sin(m\varphi_0)\sin(m\varphi)\right\}}_{= 4\pi\delta_{0n}}$$

$$= \frac{2 R r_{abs}}{D_{net}} \sum_{n=1}^{\infty} \frac{1}{\lambda_{0n}^3} \frac{J_0(\alpha_{0n} r_0) J_1(\alpha_{0n} R)}{[J_1(\lambda_{0n})]^2}.$$

A.2. A Two-dimensional Model of the Synaptic Cleft is Sufficient

The extension h of the synaptic cleft in the z-direction is more than ten times smaller than in lateral direction, so that it seems reasonable to reduce the model to a two-dimensional model of the synaptic cleft. To obtain a quantitative measure for the difference between two- and three-dimensional concentration profiles just above the PSD ($0 \leqslant z \leqslant \delta$), we integrate the three-dimensional profile over a small interval δ (located right above the post-synaptic membrane)

$$c_\delta(r,\varphi,t) = N_T p_\Phi(r,\varphi,t) \int_0^\delta \mathrm{d}z\; p_z(z,t) \quad \text{(A.3)}$$

and compare it to the two-dimensional concentration profile, given by $c_\Phi(r,\varphi,t) = N_T p_\Phi(r,\varphi,t)$. The relative deviation Λ is defined as

$$\Lambda = \frac{c_\Phi(r,\varphi,t) - c_\delta(r,\varphi,t)}{c_\Phi(r,\varphi,t)}$$

$$= -2\frac{h}{\delta}\sum_{n=1}^{\infty}\frac{(-1)^n}{n\pi}\sin\left(\frac{n\pi\delta}{h}\right)\mathrm{e}^{-\frac{n^2\pi^2}{h^2}D_{net}t},$$

and shown in Fig. 1(b) as a function of time for $\delta = 5$ nm, different heights h of the synaptic cleft and a relatively slow diffusion coefficient of $D_{net} = 30\ \mathrm{nm}^2\,\mu\mathrm{s}^{-1}$. (Larger values of the diffusion constant give rise to an even faster decay of Λ). Obviously the difference between a three- and a two-dimensional model of the synaptic cleft vanishes within a few microseconds. This indicates that we find a stationary state in the z-direction within microseconds, which is very fast compared with the time-scale of receptor kinetics ($\sim$ms), and hence rationalizes our approach to use a two-dimensional model.

A.3. Calculation of the Time-dependent Local Transmitter Concentration

We consider a distribution of receptors exposed to the spatio-temporal concentration profile $c(\mathbf{r},t)$ from eqn (A.2). In the simplest case the transmitter molecules are released in the middle of the synaptic disc, so that

$$c(\mathbf{r},t) = \frac{N_T}{\pi r_{abs}^2}\sum_{n=1}^{\infty}\frac{J_0(\alpha_{0n}|\mathbf{r}|)}{[J_1(\lambda_n)]^2}\,\mathrm{e}^{-\alpha_{0n}^2 D_{net}t}.$$

The receptor i at position $\mathbf{r}_i$ is exposed to a local concentration $C_i^{(\Delta F)}(t)$, which is estimated by integrating $c(\mathbf{r},t)$ over the small area increment ΔF around $\mathbf{r}_i$ shown in Fig. 1. This leads to

$$C_i^{(\Delta F)}(t) = \frac{N_T}{r_{abs}^2}\frac{\Delta\varphi}{\pi}\sum_{n=1}^{\infty}\left\{\frac{(r_i+\varepsilon)J_1[\alpha_n(r_i+\varepsilon)]}{\alpha_n[J_1(\lambda_n)]^2} - \frac{(r_i-\varepsilon)J_1[\alpha_n(r_i-\varepsilon)]}{\alpha_n[J_1(\lambda_n)]^2}\right\}\mathrm{e}^{-\alpha_n^2 D_{net}t}. \quad \text{(A.4)}$$

The local concentration in mM then determines the transition rates according to*

$$\tilde{k}_i = k_i\frac{C_i^{(\Delta F)}(t)}{\Delta F\ h\ N_A}. \quad \text{(A.5)}$$

*A larger diffusion coefficient speeds up the equilibration of transmitter across the PSD and further reduces the influence of spatially different receptor arrangements.

A.4. Set of Kinetic Differential Equations for a Single Receptor in a Local Time-dependent Concentration Field

The receptor i at position $\mathbf{r}_i$ is exposed to the local time-dependent transmitter concentration $C_i^{(\Delta F)}(t)$. Average properties, like the average probability of receptor i to be in the open state $C4$ can be calculated from a set of chemical kinetic (master) equations (Gardiner, 1983), which describe the dynamic evolution of the probabilities $P_\alpha^{(i)}$ for receptor i to be in state α:

$$\begin{aligned}
\frac{\mathrm{d}}{\mathrm{d}t}P_{C0}^{(i)} &= -\tilde{k}_{+1}P_{C1}^{(i)} + k_{-1}P_{C2}^{(i)}\\
\frac{\mathrm{d}}{\mathrm{d}t}P_{C1}^{(i)} &= \tilde{k}_{+1}P_{C0}^{(i)} - \left\{k_{-1} + \tilde{k}_{+2} + \alpha_1\right\}P_{C1}^{(i)} + k_{-2}P_{C2}^{(i)} + \beta_1 P_{C3}^{(i)}\\
\frac{\mathrm{d}}{\mathrm{d}t}P_{C2}^{(i)} &= \tilde{k}_{+2}P_{C1}^{(i)} - \left\{k_{-2} + \alpha + \alpha_2\right\}P_{C2}^{(i)} + \beta P_O^{(i)} + \beta_2 P_{C4}^{(i)}\\
\frac{\mathrm{d}}{\mathrm{d}t}P_{C3}^{(i)} &= \alpha_1 \mathrm{P}_{C1}^{(i)} - \left\{\beta_1 + \tilde{k}_{+3}\right\}P_{C3}^{(i)} + k_{-3}P_{C4}^{(i)}\\
\frac{\mathrm{d}}{\mathrm{d}t}P_{C4}^{(i)} &= \tilde{k}_{+3}P_{C3}^{(i)} + \alpha_2 P_{C2}^{(i)} - \left\{k_{-3} + \beta_2 + \alpha_4\right\}P_{C4}^{(i)} + \beta_4 P_{C5}^{(i)}\\
\frac{d}{dt}P_{C5}^{(i)} &= \alpha_4 P_{C4}^{(i)} - \left\{\beta_4 + \beta_3\right\}P_{C5}^{(i)} + \alpha_{+3}P_O^{(i)}\\
\frac{\mathrm{d}}{\mathrm{d}t}P_O^{(i)} &= \alpha P_{C2}^{(i)} - \left\{\beta + \alpha_3\right\}P_O^{(i)} + \beta_3 P_{C5}^{(i)}.
\end{aligned} \quad \text{(A.6)}$$

For definition of receptor states and transition rates see Fig. 4. Each receptor has to be in one of its available states, so that

$$P_{C1}^{(i)} + P_{C2}^{(i)} + P_{C3}^{(i)} + P_{C4}^{(i)} + P_{C5}^{(i)} + P_{C6}^{(i)} + P_O^{(i)} = 1$$

holds.

After specifying the initial conditions, here $P_{C1}^{(i)} = 1$ and $P^{(i)} = 0$ for all other states—all receptors are initially in the closed unbound state—the set of eqns (A.6) is solved numerically for each receptor. This yields for instance the open probability $P_O^{(i)}(t)$ of each of the n_{rec} receptors, which can then be averaged to gain the total, averaged synaptic response of the receptor population

$$P_O^{(tot)}(t) = \frac{1}{n_{rec}}\,\Sigma_{i=1}^{n_{rec}}\,P_O^{(i)}(t).$$